THE HEIGHT DIGITAL IMAGE CORRELATION (hDIC) TECHNIQUE FOR THE IDENTIFICATION OF TRIAXIAL SURFACE DEFORMATIONS

Fatih Uzun[1,2], Alexander M Korsunsky[1,3,*]

[1]MBLEM, Department of Engineering Science, The University of Oxford

[2]fatihuzun@me.com, fatih.uzun@eng.ox.ac.uk

[3]alexander.korsunsky@eng.ox.ac.uk, [*]corresponding author

Authors' Accepted Manuscript

Published version in *International Journal of Mechanical Sciences*

Volume 159, 2019, Pages 417-423

https://doi.org/10.1016/j.ijmecsci.2019.06.014

ABSTRACT

This paper introduces the height digital image correlation (hDIC) technique for the identification of triaxial deformations. Conventional digital image correlation (DIC) uses pixel image intensity as the basis for the determination of in-plane displacement fields. We demonstrate the advantages of using the out-of-plane surface height and its variation during deformation to extract information about triaxial (in-plane and out-of-plane) displacement fields. Surface height maps can be obtained by optical profilometry or scanning probe microscopies, e.g. stylus profilometry, coordinate measurement machine (CMM), or atomic force microscope (AFM). The changes in height during deformation are sufficiently small to allow efficient correlation of in-plane displacements with sub-pixel accuracy, yet also provide information about out-of-plane displacements. In the present study, the contour map of surface height was created using digital dynamic focus optical microscope. The correlation between the reference and target maps to extract the displacement data was accomplished by a two-step correlation process. Initially, triaxial Cartesian coordinate data of reference and target data sets were cross-correlated at integer-pixel level sensitivity. This was followed by sub-pixel correlation using gradient descent method. As an example of technique application, Al alloy test specimens were subjected to large tensile deformations to failure. Good agreement was found between height digital image correlation (hDIC) analysis of displacements and strains and the reference material properties, with the evolution of both in-plane strains and out-of-plane displacements show progressive localisation during post-critical deformation beyond the sample's ultimate tensile strength (UTS).

Keywords: height digital image correlation; triaxial deformations; surface contour; integer-pixel level cross-correlation; sub-pixel level correlation

1. INTRODUCTION

Digital Image Correlation (DIC) technique was introduced by Parks [1] in 1982 to measure deformations using speckle photography. Chu et. al [2] presented applications of the digital speckle patterns on experimental mechanics in 1985. During the following decades, improvements in digital imaging technologies and processing units of computers led to new insights. Full-field digital imaging became widely used when deformation could not be monitored using classical contact-based experimental methods [3]. Today, the applications of DIC and Digital Volume Correlation (DVC) vary from the evaluation of 2D and 3D displacements at the surface of solids [4] to the determination of volumetric deformations inside large components [5].

Biaxial deformations on a flat surface are determined using 2D-DIC without requirement of initial image processing while stereo 3D-DIC first transforms different image data sets into a plane using image registration algorithms [6]. They are used for quantification of 2D and 3D deformations [7]. Stereo 3D-DIC methods are based on surface triangulation and allow depth measurements [8] and 3D surface reconstruction of objects [9]. These are widely used for correlation analysis of displacement over large areas. However, the precision of surface displacement determination obtained using surface triangulation methods are far from nano-level precision. Digital volume correlation (DVC) is an extension of conventional DIC [10] for determination of volumetric deformations that uses X-Ray tomography images. Triaxial in-volume deformations within a body can be calculated using DVC, but it requires costly imaging procedures and high computational power.

Digital microscopy images have been used since the early times of the introduction of DIC technique. Different DIC systems that combine metallurgical microscopes with charge coupled devices (CCDs) were used for the determination of surface deformations [11–13]. Scanning Tunneling Microscopy and Atomic Force Microscopy were used for the correlation of topographic images to map deformations with nano-scale precision [14–16] over small areas, but the use of topography information for the determination of out-of-plane deformations of large areas with micro- and nano-scale precision has remained missing.

Two widely used surface DIC algorithms are local DIC and global DIC algorithms [6]. Local DIC uses local subsets to determine the deformations in each subset individually [17], while global DIC calculates the deformations in the entire surface simultaneously [18]. Local DIC algorithms are composed of integer-pixel level search and sub-pixel level search stages. HajiRassouliha et. al [19] classified algorithms corresponding to these stages as the integer shift and the sub-pixel shift algorithms. The integer shift algorithms are cross-correlation [20], normalized cross-correlation [21], phase-correlation [22], gradient-correlation [23] and normalized gradient-correlation [24] and the sub-pixel shift algorithms are interpolation in spatial domain [25], interpolation in frequency domain [25], curve fitting [26], analytical solution [27] and phase-based method [20]. Bing et. al [28] and Hu et. al [7] analysed performance of sub-pixel level search algorithms for 2D and 3D-DIC respectively. According to these studies, commonly used sub-pixel level DIC algorithms are intensity interpolation, which is known as the coarse-fine search method [29], Newton-Raphson iteration [17,30] and gradient based methods [31]. Among these algorithms, Newton-Raphson is observed to have the highest accuracy in both studies [7,28]. Both gradient based methods and Newton-Raphson iteration starts with an initial guess, but insufficiently precise initial guess can lead to incorrect solution. Gradient descent method uses first order derivatives while Newton-

Raphson method needs solving first and second order derivatives. In addition, gradient descent method uses higher number of iterations that require less computation power and memory when compared to the Newton-Raphson method.

Current DIC methods that aim to determine out-of-plane displacements are limited to either very high-resolution analysis over small areas, or low resolution and low precision mapping over large areas. In this study, we propose and demonstrate a method that fills the gap between previous approaches. The height Digital Image Correlation (hDIC) method is capable of out-of-plane displacement mapping over small and large areas with micro-level resolution (in plane) and nano-scale precision. Furthermore, micro-scale in-plane displacement information is also extracted, thus providing a method for large area, high precision triaxial displacement DIC mapping. The proposed method is based on the correlation of height contour data measured using highly sensitive digital optical microscopy techniques with height profilometry capability. Pixels are defined in terms of height information rather than image intensity. The normal to surface components of the contour data of the deformed condition is correlated with the corresponding data in the reference condition through a two-level correlation procedure. The process begins with integer-pixel level cross-correlation. Subsequent to the determination of initial matching coordinates, gradient descent method is used for sub-pixel level correlation to assess triaxial deformations with high precision. Accuracy of the proposed method is analysed by *in situ* investigation of elastic stage of the tensile test of aluminium specimen and triaxial deformations are calculated in three main steps of the same tensile test.

2. HEIGHT DIGITAL IMAGE CORRELATION (hDIC)

In a recent study, Dave et. al [32] used The Alicona InfiniteFocus instrument for investigating inter- and intra-granular deformations. This instrument is capable of capturing high resolution images from non-flat surfaces by performing height scanning of the sample and identifying in-focus regions at each height. Thus, the device is able to determine sample surface profile. The use of microscopy images for the purpose of determination of planar displacements is a well-known process, but the benefit of the third component of contour data has not been used for the determination of out-of-plane deformations with micro-level resolution and nano-scale precision, because the conventional DIC is based on image intensity analysis. The proposed hDIC method uses triaxial Cartesian coordinates of the surface for the purpose of determination of complete displacement vector of planar surfaces.

Similar to the conventional DIC, the objective of hDIC is to capture deformations in the region of interest (ROI). Speckle patterns used in conventional DIC is replaced by height patterns from optical microscopy corresponding to each coordinate on the planar surface of reference and target conditions. The use of pure triaxial Cartesian coordinate data eliminates the requirement of a calibration process. The correlation process is composed of two stages which are integer-pixel level cross-correlation and sub-pixel level correlation.

2.1. Integer-Pixel Level Cross-Correlation

The integer-pixel level cross-correlation process matches the subsets in a predetermined interval. Subsets of pixels in the region of interest of reference body are created in square

form with a dimension of $(2N+1) \times (2N+1)$ where N is an integer constant [28]. The best matching subset is searched in the target as illustrated in Figure 1.

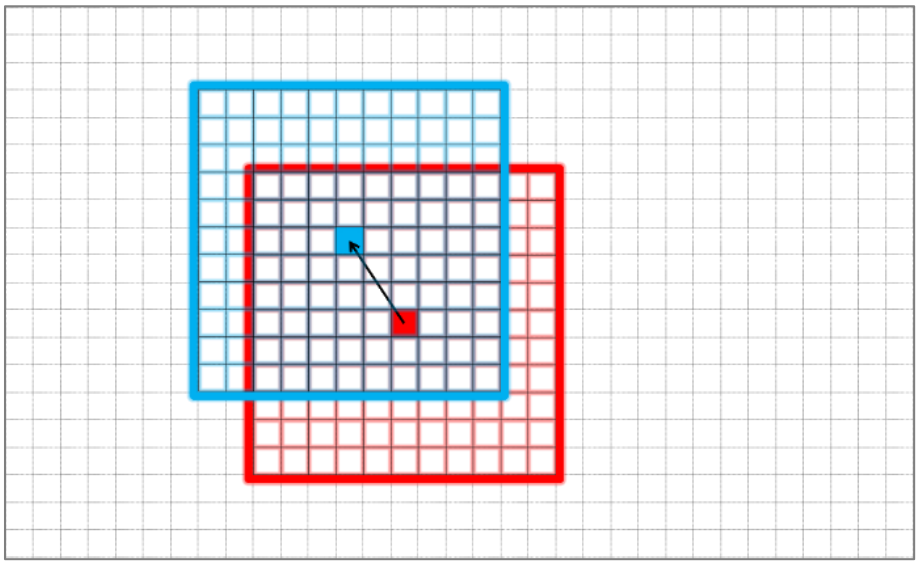

Figure 1. Illustration of integer-pixel level cross-correlation of subset with 121 (11×11) pixels. The illustration includes pixels and subsets. Reference subset is illustrated in red-grid and target subset is represented in blue-grid.

Pan et. al [33] showed that the similarity between reference and target subsets are the same after their investigations on three different cross-correlation criteria. Based on the outcomes of that study, the zero-mean normalised cross-correlation method, which is given in Equation 1, is used for the matching process. In this equation, C_i is the cross-correlation coefficient of i^{th} subset, $R(x,y)$ is the intensity of the pixel at coordinates (x,y) in the reference subset, $T(x',y')$ is the intensity of the pixel at coordinates (x',y') in the target subset, R_m is the mean intensity of the pixels in the reference subset and T_m is the mean intensity of the pixels in the target subset.

$$C_i = \frac{\sum(R(x,y) - R_m)(T(x',y') - T_m)}{\sqrt{\sum(R(x,y) - R_m)^2}\sqrt{\sum(T(x',y') - T_m)^2}} \quad (1)$$

Coordinates of a pixel in the target plane are determined using Equation 2 where u represents the displacement in *x*-axis and v represents the displacement in *y*-axis. Different than the conventional DIC methods, first or second order approximation procedures are not applied, because the aim of integer-pixel level cross-correlation process is the determination of initial estimated coordinates for sub-pixel level correlation.

$$x' = x + u(x,y) \quad (2a)$$

$$y' = y + v(x,y) \quad (2b)$$

2.2. Sub-Pixel Level Correlation

Gradient descent is one of the well-known optimization methods which was invented by Cauchy [34] to find the minimum of multi-variable functions that never becomes zero within a given interval. This method is based on determination of gradient of a function starting from the initial guess point and iterating the process in the negative direction of the gradient until the gradient vanishes. In this study, subsequent to the initial estimation of the coordinates of matching subsets in the target data, sub-pixel level correlation is performed using gradient descent method.

The pixel intensities in the target are fitted to a two dimensional function, $F_T(x', y')$, using a bi-cubic interpolation process based on the formulation given in Equation 3 to calculate the pixel intensity of the matching pixel at coordinates (x', y') in the target subset where $\omega_{i,j}$ is

the coefficient in the dimensions of i and j. The final equation distributes on grid surface of unit squares and it has continuous derivatives [35].

$$F_T(x', y') = \sum_{i=0}^{3} \sum_{j=0}^{3} \omega_{i,j} (x')^i \, (y')^j \tag{3}$$

Sub-pixel level correlation process determines the best matching point in the target function through a pixel by pixel analysis. This necessitates the determination of the cost function of sub-pixel level correlation process for each reference pixel separately using Equation 4 given below.

$$J(x, y) = \left(F_T(x', y') - \ R(x, y)\right)^2 \tag{4}$$

Gradient decent minimization process simultaneously updates the x' and y' coordinates in the target function along the steepest descent direction using Equation 5. In this equation α represents the step size which is kept as a constant positive number throughout the process.

$$x' \coloneqq x' - \alpha \frac{\partial}{\partial x'} J(x', y') \tag{5a}$$

$$y' \coloneqq y' - \alpha \frac{\partial}{\partial y'} J(x', y') \tag{5b}$$

3. *IN SITU* MONITORING OF TRIAXIAL DEFORMATIONS

The proposed hDIC method was used for monitoring the tensile test of an aluminium dog-bone specimen. Microscopic contour data sets were recorded from different steps of the

tensile test in order to analyse sub-pixel level correlation accuracy and determine triaxial deformations. 15 microscopic scans were performed in the region of interest for the determination of height variations. Initial scan was performed for obtaining reference contour data before loading. 7 scans were performed in the elastic region of the tensile test for the analysis of sub-pixel level correlation accuracy and 7 scans were performed in the plastic range for the investigation of triaxial deformations.

hDIC correlations were performed using reference and target data sets of height intensities which were measured with a sensitivity of 8 µm. Subsets used for the hDIC correlation were composed of 121 (11×11) pixels. No interval was left between subsets of the reference state and correlations were performed for each pixel individually. The distribution of height coordinates in a subset with 121 pixels whose centre is located at x and y coordinates of -5575 and -1102 µm respectively in the reference data set is illustrated in Figure 2.

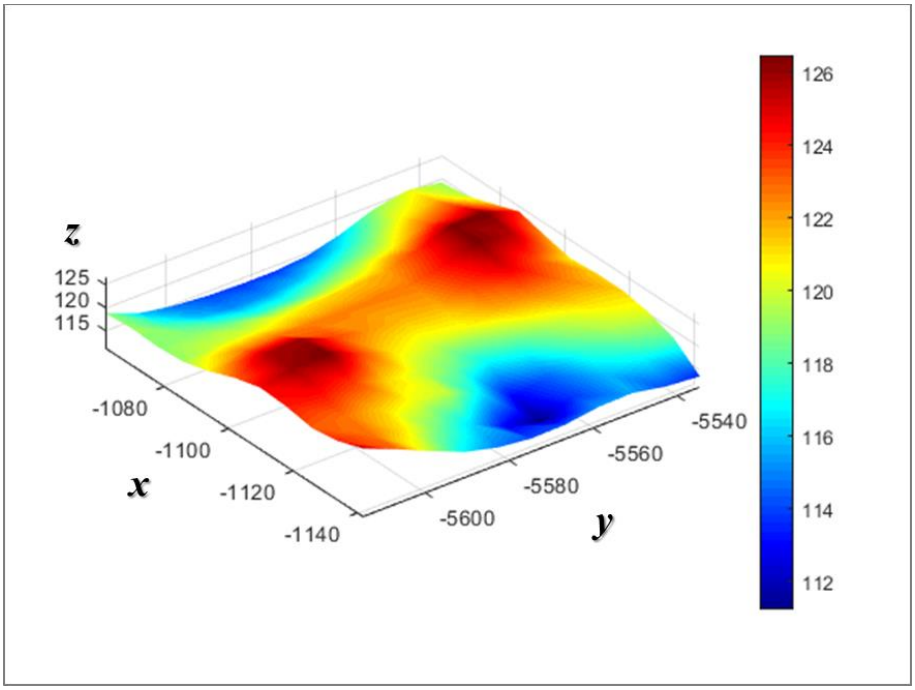

Figure 2. Distribution of height data (micrometre) in a subset located in the reference data set.

3.1. Sample Preparation and Experimental Setup

Tensile test specimens were prepared using HE 30 6082 aluminium that has 70 GPa elastic modulus and 0.33 Poisson's ratio [36] according to the data provided by manufacturers. Side and surface cuts were created using electric discharge machining technique. This technique is based on creating electric arc that causes formation of pits with a depth of a few micron on the cut surface. Height data corresponding to the hills and valleys that are created by the pits was collected by the Alicona Infinite Focus 3D Profilometer instrument. Vertical and lateral resolutions for the scanning process were determined to be 200 nm and 6 μm respectively. This device has a potential to reach 10 nm resolution that is sufficiently enough for obtaining all details about surface roughness, which can be used for the purpose of correlation, even on the polished surfaces. However, scanning large areas at very high resolutions requires hours of scanning time and creates immensely large amount of data that requires high cost computational processes for the analysis. Accordingly, the capability of the hDIC method on the determination of triaxial deformations was investigated on a surface that has very high surface roughness, which was created by the EMD cutting technique.

5kN tensile stage produced by Deben UK is used for tensile test. The microscopy image of the reference data, the region of interest and dimensions of the dog bone specimen are illustrated in Figure 3. Thickness of the specimen is 2 mm. Microscopy scans cover an area that exceeds the dimensions of the gauge. The region of interest has the same width with the gauge, but its length is determined to be 8 mm, and both the dog bone specimen and the region of interest have the same centre on the 2-dimensional plane.

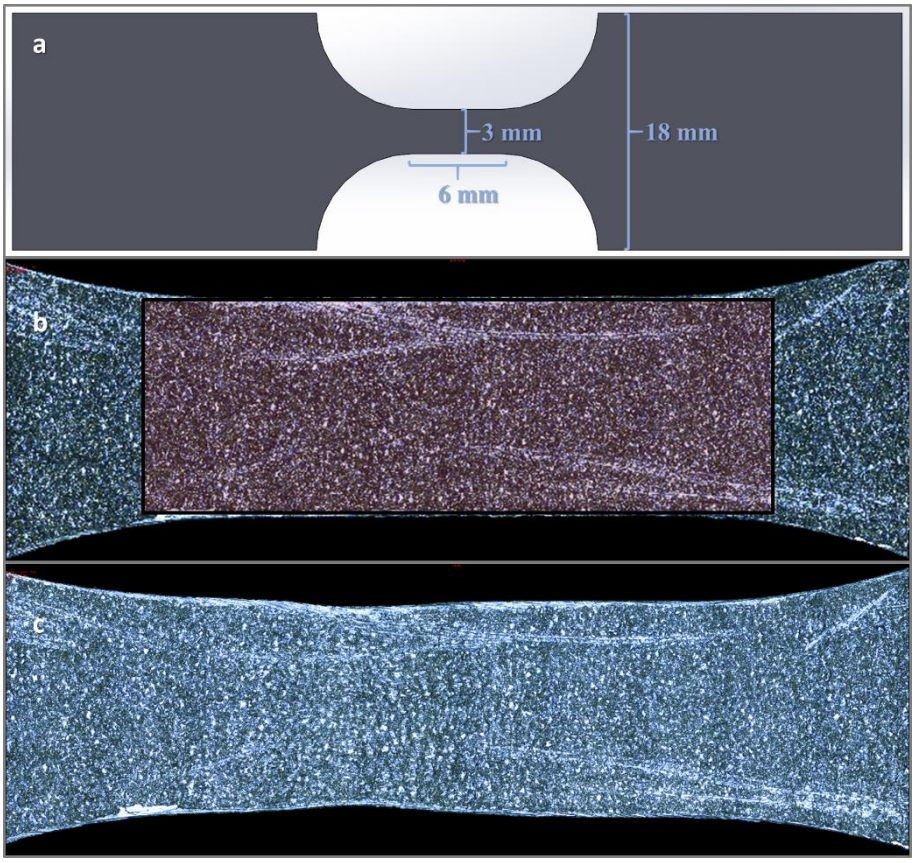

Figure 3. The dimensions (a) and microscopy images of HE 30 6082 dog-bone tensile test specimen at the reference state (b) with the region of interest (ROI) and at the final state before break (c).

Among 7 measurement steps of plastic stage, results were analysed at 3 steps of plastic stage of tensile test which are the beginning of plastic stage, the ultimate tensile strength and final step immediately before break. The surface height data of stress-free reference condition and 3 steps of plastic stage of tensile test are illustrated in Figure 4. Plastic-A represents the beginning of plastic stage, Plastic-B represents the step where ultimate tensile strength is reached, and Plastic-C represents the step before break. Microscopy based contour measurements show that the surface height decreases at around the necking zone.

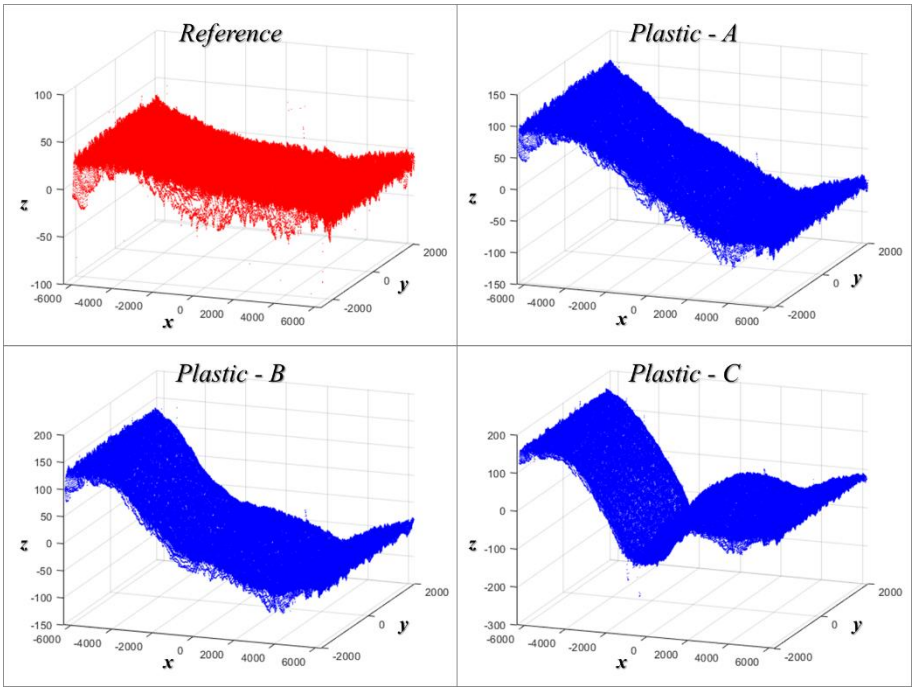

Figure 4. The surface contour data (micrometre) of stress-free reference condition and 3 steps of plastic stage of tensile test.

3.2. The hDIC Sub-Pixel Level Correlation Accuracy

Accuracy of sub-pixel level correlation process was analysed using the correlation of 7 different steps of the elastic stage of tensile test. This analysis was done based on the fact that unit displacement during the tensile test is directly proportional with the distance from the centre of the dog-bone specimen. The strength of linearity between the hDIC displacement calculations and their location along the longitudinal length of the dog-bone specimen were determined. The Pearson coefficients of each step were calculated using displacements corresponding to the pixels in the region of interest. Distribution of linear correlation of displacements averaged through the long-transverse direction along the longitudinal position are given in Figure 5. Throughout the text, long-transverse represents the width and short-transverse represents the thickness.

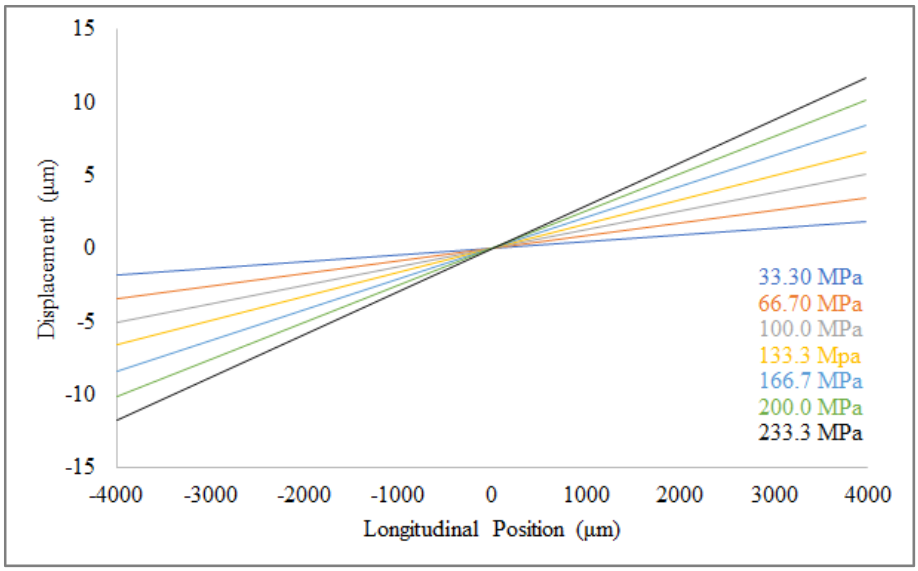

Figure 5. Linear correlations of longitudinal x-component of displacements with respect to their longitudinal position.

The average of Pearson coefficients, that were determined for all steps of elastic stage, was calculated as 0.9989. It can be concluded that displacements have linear relation with distance from the centre of the dog-bone specimen in all loading steps. Very high strength of linearity shows that the hDIC sub-pixel level correlation process has a high accuracy.

3.3. Determination of Triaxial Deformations

During the elastic stage, the true stress increases rapidly and yielding starts after a certain magnitude of stress. Yibo et. al. [37] state that the increase of true stress in the plastic stage is much slower than the elastic stage and strain increases with an increasing rate during plastic stage. The flow stress, which is the true stress in the plastic range, increases until the necking gets appeared at stress values close to ultimate tensile strength. At that stage, triaxial strains around neck increases at a much higher rate when compared to the whole gauge volume. In this study, the hDIC sub-pixel level correlation process was used to determine the triaxial

deformations before and after the necking at 7 different loading steps of yield stage of tensile test.

Figure 6 illustrates longitudinal x-, long-transverse y- and short-transverse z-component of displacements for 3 main stages of plastic stage. x-displacements get a homogeneous distribution along the transversal direction with increasing magnitude. y-displacements in all stages of plastic deformation show formation of the neck. z-displacements in the necking zone increase with the increasing extension along the longitudinal direction. The steps before and after the break have highest z-displacement magnitudes.

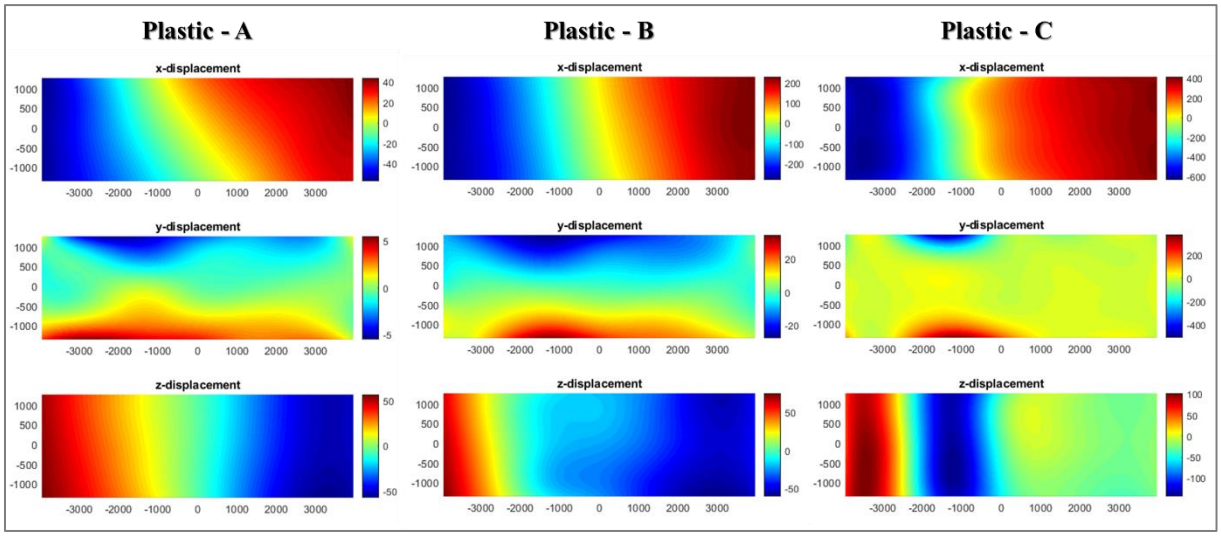

Figure 6. Illustration of longitudinal x-, long-transverse y- and short-transverse z-component of displacements at 3 steps of plastic stage of tension test.

3.4. Determination of Strains and Mechanical Properties

Longitudinal x- and long-transverse y-components of the strain were calculated within the region of interest by differentiating the functions $f_u(x, y)$ and $f_v(x, y)$, created by bi-cubic interpolation of displacements, with respect to the corresponding displacement component

using Equations 6a and 6b. In these equations ε_x and ε_y represents longitudinal x- and short-transverse y-component of strain.

$$\varepsilon_x = \frac{\partial f_u(x,y)}{\partial x} \tag{6a}$$

$$\varepsilon_y = \frac{\partial f_v(x,y)}{\partial y} \tag{6b}$$

The relation between longitudinal stress and longitudinal strain is illustrated in Figure 7. Strains were calculated as average strain within the region of interest. In this plot, A represents the first step of plastic range, B represents the ultimate tensile strength and C represents the end of yield stage before break. Yield strength and ultimate tensile strength for the test specimen were determined as 266 and 293 MPa respectively which are in good agreement with the literature properties of this material [36].

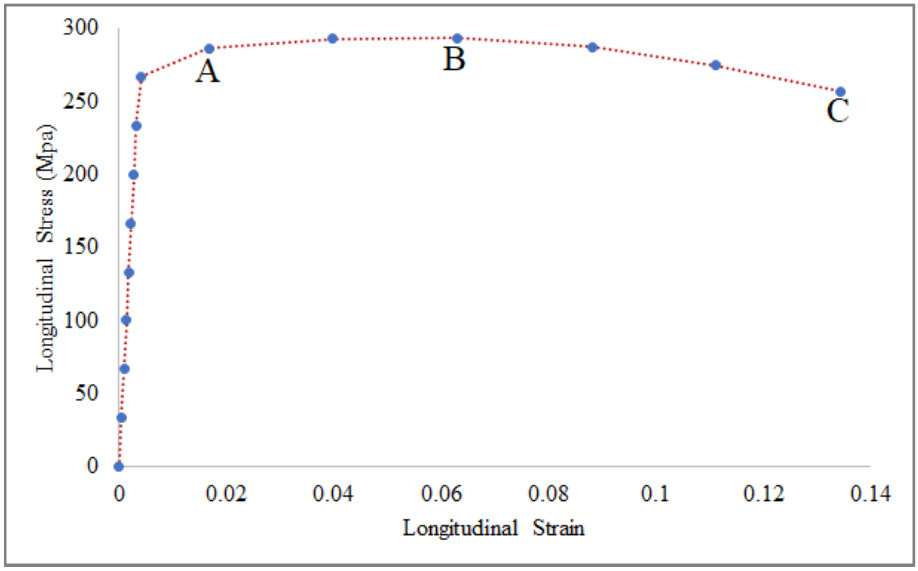

Figure 7. The relation between longitudinal stress and longitudinal strain calculated using hDIC.

The slope of longitudinal and long-transverse stress strain-plots in the elastic region are illustrated in Figures 8a and 8b. The slopes of these plots are 73 and -239 GP for longitudinal and long-transverse directions respectively. Modulus of elasticity of the HE 30 6082 aluminium specimen was calculated using the slope of longitudinal stress strain plot. Negative of the ratio between the slopes of longitudinal and long-transversal stress strain-plots, that gives the Poisson's ratio, was calculated as 0.30561. It can be stated that calculated modulus of elasticity and Poisson's ratio from these plots are in good agreement with literature values [36] of this material.

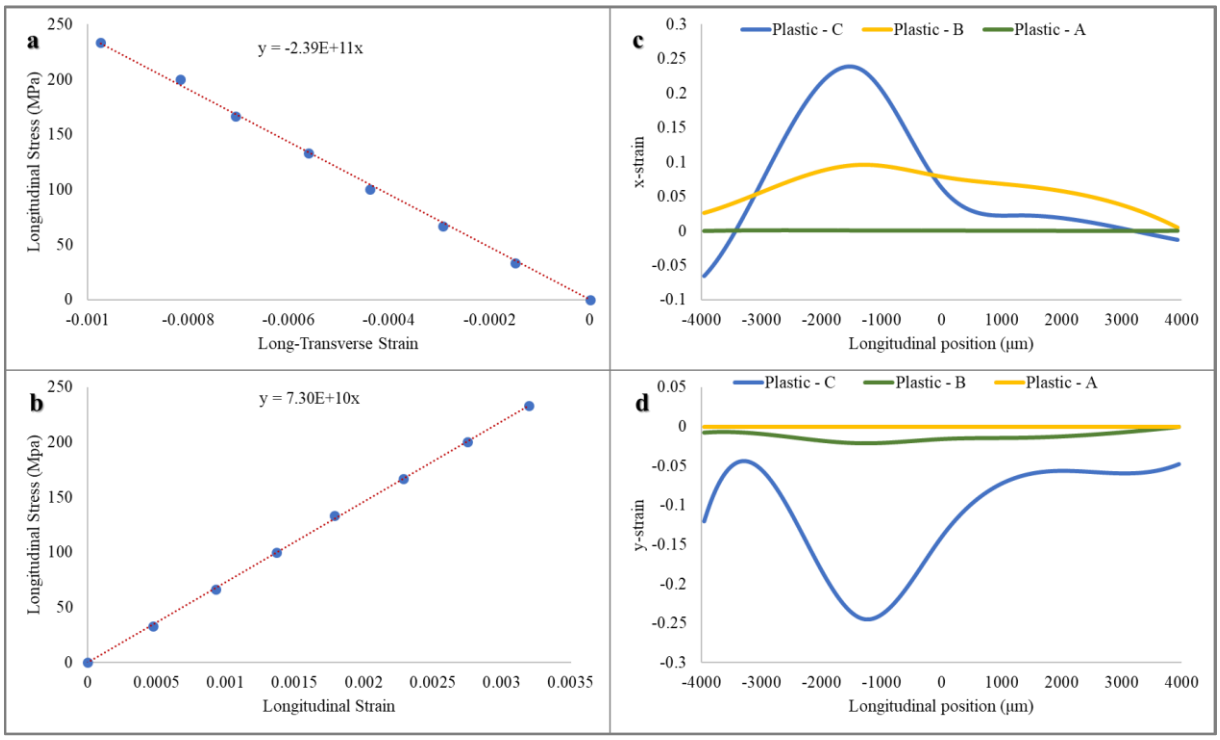

Figure 8. Averaged long-transverse (a) and longitudinal (b) strains at different stress steps of elastic stage of tension test and longitudinal (c) and long-transverse (d) strains averaged through the long-transverse direction at three different steps of plastic stage.

Figures 8c and 8d show that strains are higher at around the necking zone and it is observed that strain relaxation occurs at yield-C step. The relaxation of strain energy, after a high

increase of strain energy in the necking zone, took place in the whole specimen during the last step of plastic deformation before the break.

Strain results in Figure 9 show that the magnitude and distribution of strains around the necking zone increase after each loading step. Korsunsky and Kim [38] previously investigated the essential work of tearing using a single test specimen of HS 30 6082 aluminium and showed that the essential work of fracture is proportional with the ligament length. Studies on the essential work of plane stress in ductile materials [39] also showed that plastic strain rate is much higher in the necking zone. Similarly, strain distributions given in Figure 9 proves that the proposed hDIC method is capable of mapping the strains formed during the necking. As it is expected, longitudinal strains are tensile and long-transverse strains are compressive in the necking zone.

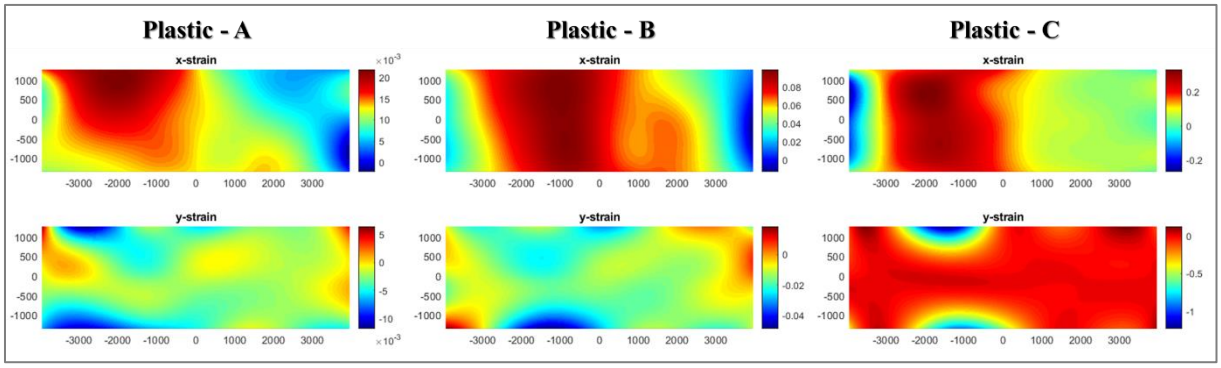

Figure 9. Distribution of longitudinal x- and long-transverse y-component of strains at 3 steps of plastic stage of tension test.

4. CONCLUSION

The hDIC technique for the determination of triaxial displacements on the surface of deformed materials is introduced. This technique is based on correlation of out-of-plane

contour coordinates of surface roughness data in spite of pixel intensity of digital images. The hDIC technique uses subsets for integer-pixel level cross-correlation and performs sub-pixel level correlation using gradient descent method for all pixels in the region of interest. The proposed approach allows determination of out-of-plane deformations in the target condition without requirement of series of digital images. The example application to one of the basic solid mechanics problems showed that the hDIC technique is effective on the determination of both short- and long-range deformations successfully.

ACKNOWLEDGEMENTS

This project has received funding from the European Union's Horizon 2020 research and innovation programme under the Marie Sklodowska-Curie grant agreement No 794957 and EPSRC through grant EP/S005072/1 Strategic Partnership in Computational Science for Advanced Simulation and Modelling of Engineering Systems (ASiMoV).

REFERENCES

[1] Parks VJ. The range of speckle metrology. Exp Mech 1980;20:181–91. https://doi.org/10.1007/BF02327597.

[2] Chu TC, Ranson WF, Sutton MA. Applications of digital-image-correlation techniques to experimental mechanics. Exp Mech 1985;25:232–44. https://doi.org/10.1007/BF02325092.

[3] Hild F, Roux S. Digital image correlation: From displacement measurement to identification of elastic properties - A review. Strain 2006;42:69–80. https://doi.org/10.1111/j.1475-1305.2006.00258.x.

[4] Zhao P, Zsaki AM, Nokken MR. Using digital image correlation to evaluate plastic shrinkage cracking in cement-based materials. Constr Build Mater 2018;182:108–17. https://doi.org/10.1016/j.conbuildmat.2018.05.239.

[5] Zhong FQ, Indurkar PP, Quan CG. Three-dimensional digital image correlation with improved efficiency and accuracy. Meas J Int Meas Confed 2018;128:23–33. https://doi.org/10.1016/j.measurement.2018.06.022.

[6] Wang B, Pan B. Subset-based local vs. finite element-based global digital image correlation: A comparison study. Theor Appl Mech Lett 2016;6:200–8. https://doi.org/10.1016/j.taml.2016.08.003.

[7] Hu Z, Xie H, Lu J, Hua T, Zhu J. Study of the performance of different subpixel image correlation methods in 3D digital image correlation. Appl Opt 2010;49:4044–51. https://doi.org/10.1364/AO.49.004044.

[8] Pan B, Yu LP, Zhang QB. Review of single-camera stereo-digital image correlation techniques for full-field 3D shape and deformation measurement. Sci China Technol Sci 2018;61:2–20. https://doi.org/10.1007/s11431-017-9090-x.

[9] Prakoonwit S, Benjamin R. 3D surface reconstruction from multiview photographic images using 2D edge contours. 3D Res 2012;3:1–12. https://doi.org/10.1007/3DRes.04(2012)6.

[10] Bay BK, Smith TS, Fyhrie DP, Saad M. Digital volume correlation: Three-dimensional strain mapping using x-ray tomography. Exp Mech 1999;39:217–26. https://doi.org/10.1007/BF02323555.

[11] Sutton M, Mingqi C, Peters W, Chao Y, McNeill S. Application of an optimized digital correlation method to planar deformation analysis. Image Vis Comput 1986;4:143–50. https://doi.org/10.1016/0262-8856(86)90057-0.

[12] Sun Z, Lyons JS, McNeill SR. Measuring Microscopic Deformations with Digital

Image Correlation. Opt Lasers Eng 1997;27:409–28. https://doi.org/10.1016/S0143-8166(96)00041-3.

[13] Luo M. Displacement/strain measurements using an optical microscope and digital image correlation. Opt Eng 2006;45:033605. https://doi.org/10.1117/1.2182108.

[14] Li X, Xu W, Sutton MA, Mello M. Nanoscale deformation and cracking studies of advanced metal evaporated magnetic tapes using atomic force microscopy and digital image correlation techniques. Mater Sci Technol 2006;22:835–44. https://doi.org/10.1179/174328406x101283.

[15] Sun Y, Pang JHL, Fan W. Nanoscale deformation measurement of microscale interconnection assemblies by a digital image correlation technique. Nanotechnology 2007;18. https://doi.org/10.1088/0957-4484/18/39/395504.

[16] Xu ZH, Sutton MA, Li X. Mapping nanoscale wear field by combined atomic force microscopy and digital image correlation techniques. Acta Mater 2008;56:6304–9. https://doi.org/10.1016/j.actamat.2008.08.044.

[17] Bruck HA, McNeill SR, Sutton MA, Peters WH. Digital image correlation using Newton-Raphson method of partial differential correction. Exp Mech 1989;29:261–7. https://doi.org/10.1007/BF02321405.

[18] York N, Sun Y, Pang JHL, Wong CK, Su F. Finite element formulation for a digital image correlation method. Appl Opt 2005;44:7357–63. https://doi.org/10.1364/AO.44.007357.

[19] HajiRassouliha A, Taberner AJ, Nash MP, Nielsen PMF. Subpixel phase-based image registration using Savitzky–Golay differentiators in gradient-correlation. Comput Vis Image Underst 2018;170:28–39. https://doi.org/10.1016/j.cviu.2017.11.003.

[20] Malcolm DTK, Nielsen PMF, Hunter PJ, Charette PG. Strain measurement in biaxially loaded inhomogeneous , anisotropic elastic membranes. Biomechan Model

Mechanobiol 1 2002;1:197–210. https://doi.org/10.1007/s10237-002-0018-8.

[21] Debella-Gilo M, Kääb A. Sub-pixel precision image matching for measuring surface displacements on mass movements using normalized cross-correlation. Remote Sens Environ 2011;115:130–42. https://doi.org/doi.org/10.1016/j.rse.2010.08.012.

[22] Alba A, Aguilar-Ponce RM, Vigueras-Gómez JF, Arce-Santana E. Phase Correlation Based Image Alignment with Subpixel Accuracy. In: Batyrshin I, González Mendoza M, editors. Adv. Artif. Intell., Berlin, Heidelberg: Springer Berlin Heidelberg; 2013, p. 171–82.

[23] Neggers J, Blaysat B, Hoefnagels JPM, Geers MGD. On image gradients in digital image correlation. Int J Numer Methods Eng 2016;105:243–60. https://doi.org/10.1002/nme.4971.

[24] Tzimiropoulos G, Argyriou V, Stathaki T. Subpixel registration with gradient correlation. IEEE Trans Image Process 2011;20:1761–7. https://doi.org/10.1109/TIP.2010.2095867.

[25] Póth M, Szakáll T. Spatial and Frequency Domain Comparison of Interpolation Techniques in Digital Image Processing, 2009.

[26] Nobach H, Honkanen M. Two-dimensional Gaussian regression for sub-pixel displacement estimation in particle image velocimetry or particle position estimation in particle tracking velocimetry. Exp Fluids 2005;38:511–5. https://doi.org/10.1007/s00348-005-0942-3.

[27] Foroosh H, Zerubia JB, Berthod M. Extension of phase correlation to subpixel registration. IEEE Trans Image Process 2002;11:188–200. https://doi.org/10.1109/83.988953.

[28] Pan B, Xie HM, Xu BQ, Dai FL, Bing P, Hui-min X, et al. Performance of sub-pixel registration algorithms in digital image correlation. Meas Sci Technol 2006;17:1615–

21. https://doi.org/10.1088/0957-0233/17/6/045.

[29] Zhang ZF, Kang YL, Wang HW, Qin QH, Qiu Y, Li XQ. A novel coarse-fine search scheme for digital image correlation method. Meas J Int Meas Confed 2006;39:710–8. https://doi.org/10.1016/j.measurement.2006.03.008.

[30] Cofaru C, Philips W, Paepegem W Van. Improved Newton-Raphson digital image correlation method for full-field displacement and strain calculation. Appl Opt 2010;49:6472–84.

[31] Zhou P. Subpixel displacement and deformation gradient measurement using digital image/speckle correlation (DISC). Opt Eng 2001;40:1613. https://doi.org/10.1117/1.1387992.

[32] Dave S, Song X, Hofmann F, Dragnevski K, Korsunsky AM. Digital image correlation and finite element analysis of inter- and intra-granular deformation. Procedia Eng 2009;1:197–200. https://doi.org/10.1016/j.proeng.2009.06.046.

[33] Pan B, Xie H, Wang Z. Equivalence of digital image correlation criteria for pattern matching. Appl Opt 2010;49:5501. https://doi.org/10.1364/AO.49.005501.

[34] Cauchy A-L. Methode generale pour la resolution des systemes d'equations simultanees. Compte Rendu Des Seances L'Acad'emie Des Sci 1847;25:536–8.

[35] Russell WS. Polynomial interpolation schemes for internal derivative distributions on structured grids. Appl Numer Math 1995;17:129–71. https://doi.org/10.1016/0168-9274(95)00014-L.

[36] Ruuki. Aluminium AW 6082 T6 round 2012.

[37] Yibo P, Gang W, Tianxing Z, Shangfeng P, Yiming R. Dynamic mechanical behaviors of 6082-t6 aluminum alloy. Adv Mech Eng 2013;2013:1–8. https://doi.org/10.1155/2013/878016.

[38] Korsunsky AM, Kim K. Determination of essential work of necking and tearing from a

single tensile test. Int J Fract 2005;132:37–44. https://doi.org/10.1007/s10704-005-4483-9.

[39] Cotterell B, Reddel JK. The essential work of plane stress ductile fracture. Int J Fract 1977;13:267–77. https://doi.org/10.1007/BF00040143.